Multiphoton ionization of rare gases using multichannel-quantum-defect theory

A. L'Huillier,* X. Tang, and P. Lambropoulos
Department of Physics, University of Southern California, University Park, Los Angeles, California 90089-0484
(Received 11 August 1988)

We apply multichannel-quantum-defect theory (MQDT) to multiphoton ionization of rare gases in lowest-order perturbation theory. We determine MQDT parameters of $J=1,3$ odd-parity states, $J=0,2$ even-parity states in xenon and krypton by fitting experimental energy levels and constructing Lu-Fano plots. We present calculations of two- and three-photon ionization of xenon and krypton in the autoionization region between the two thresholds. We compare autoionization spectra and also photoelectron angular distributions to experimental data [S. T. Pratt, P. M. Dehmer, and J. L. Dehmer, Phys. Rev. A 35, 3793 (1986); J. L. Dehmer, S. T. Pratt, and P. M. Dehmer, *ibid.* 36, 4494 (1987)]. Agreement between theory and experiment is reasonable, especially for krypton.

I. INTRODUCTION

Rare-gas atoms, and in particular, xenon and krypton, are often favored subjects for experimental studies of multiphoton ionization (MPI). Until recently, most of these experiments were performed at fixed frequencies and at very high laser intensities. However, with the development of pulsed tunable uv lasers, one is now able to study in more detail the *many-electron* response of an atom exposed to an intense radiation field. Some experiments are oriented towards the spectroscopy of rare gases, the multiphoton absorption being only a means for probing states which either cannot be reached by traditional vuv absorption spectroscopy, or reveal different facets of atomic dynamics through multiphoton absorption. Thus Blazewicz *et al.*[1] have studied Rydberg series and autoionizing states in xenon and krypton through four-photon excitation, while Dehmer and co-workers[2,3] have investigated three-photon autoionization processes (line shapes and photoelectron angular distributions) in Xe and Kr. The results of Dehmer and co-workers[2,3] are discussed in some detail in this manuscript.

In other experiments, performed at higher field strengths, the radiation field begins to seriously perturb the atomic states, causing an interplay between effects due to the field and those due to the atomic structure and dynamics. Landen *et al.*,[4] for example, have studied MPI of krypton through three-photon-resonant four-photon ionization at very high laser intensities (up to 7.8×10^{13} W cm^{-2}). Hutchinson and Ness,[5] using two colors, have reported laser-induced autoionization effects in xenon. All of these works, to which must be added, of course, the numerous studies[6] on above-threshold ionization, multiple ionization, and harmonic generation (although generally performed at fixed laser frequencies), point to the need for theoretical techniques to describe multiphoton absorption in rare gases and other complex atoms.

Unfortunately, the theory of multiphoton ionization of the rare gases has remained rather underdeveloped. The approach of Kulander,[7] which consists in numerically solving the time-dependent Hartree-Fock equations, enables him to calculate high-order multiphoton ionization processes, going beyond lowest-order perturbation theory. Although this is a very valuable method, it does not provide, at least for the time being, information on the details of the atomic structure, fine-structure effects, photoelectron angular distributions, etc. Other recent *ab initio* calculations,[8,9] though limited to two-photon ionization (in the weak intensity limit), point out the role of electron correlation effects in the multiphoton absorption process. Due to the complexity of the problem, none of these approaches includes fine-structure effects, responsible for the series of autoionizing resonances between the two ionization threshold $^2P_{3/2}$, $^2P_{1/2}$ of the heavy rare gases.

Although multichannel-quantum-defect theory[10–17] (MQDT) has been extensively used in the description of photoabsorption spectra of the rare gases,[12–14] apart from an early and preliminary attempt,[18] it has not been applied to the description of multiphoton ionization spectra. In the present work, we apply MQDT to the calculation of multiphoton absorption processes in xenon and krypton. Our aim is to derive transition strengths and ionization cross sections sufficiently accurate for a realistic study of multiphoton processes in rare gases and comparison with experiments.[2–5] In this spirit, we present calculations of two- and three-photon ionization in the autoionization region between the two ionization thresholds and slightly above the second threshold. We compare some of the results to experimental three-photon autoionization spectra and photoelectron angular distributions.[2,3] Such measurements are extremely valuable for MPI calculations in relatively weak fields as they provide critical tests of the atomic structure content of the theoretical model.

We adopt the so-called "eigenchannel" formulation of Fano,[11,12] well adapted for the rare gases, since the transformation matrix $U_{i\alpha}$ (eigenvectors of the reaction matrix $\mathbf{R}$) is close to a *jj-LS* coupling transformation. We perform a MQDT analysis of the $J=1,3$ odd-parity and $J=0,2$ even-parity Rydberg series of xenon and krypton, using the graphical method developed by Lu and Fano[12–14] and the computer program of Robaux and

Aymar.[19] MPI cross sections are calculated within lowest-order perturbation theory for the radiation field, by limiting the summation over intermediate states to the discrete spectrum. The dipole matrix elements from the ground state to the $J=1$ excited states are determined by fitting to experimental oscillator strengths.[12,17] The dipole matrix elements between excited states are calculated by using MQDT wave functions, whose parameters have been determined from the analysis of experimental energy spectra.

In Sec. II we briefly review multichannel-quantum-defect theory and present the numerical methods used to calculate multiphoton ionization processes, in particular, autoionization spectra and photoelectron angular distributions. In Sec. III we present these results and their comparison to existing experimental data.[2,3]

II. THEORY

Quantum-defect theory is based on the fact that a Rydberg electron moves essentially outside the core region under the simple influence of the core Coulomb potential. The effect of short-range interactions (inside the core region) can be described by a small number of parameters, slowly varying with energy. These parameters can be determined by *ab initio* calculations[20–22] or, as in the present approach, semiempirically by analyzing available data[12–14,17] (energy levels and oscillator strengths). Since the details of the theory can be found in many papers[11,12,15,16] and reviews,[10] we present here only those equations that are necessary for the self-contained exposition and discussion of our work.

A. Review of multichannel-quantum-defect theory

The MQDT introduces different basis sets satisfying boundary conditions at infinity or near the origin. The *collision* channel wave functions Ψ_i are defined by[15]

$$\Psi_i=\chi_i(f_i\cos\pi\nu_i+g_i\sin\pi\nu_i) , \tag{1}$$

where χ_i contains the core wave function and the angular-spin part of the Rydberg electron wave function. The remaining radial part is expressed as a linear combination of regular (f_i) and irregular (g_i) Coulomb wave functions. The total energy of the atomic system is defined by

$$E_i=\varepsilon_i+I_i , \tag{2}$$

where ε_i is the electron energy and I_i the energy of the core for the ith channel.

The f_i and g_i Coulomb wave functions are defined to be energy normalized for positive energies. (They correspond to the s,c wave functions of Seaton.[10]) The asymptotic behavior of Ψ_i for $\varepsilon_i\geq 0$ is

$$\Psi_i\sim\chi_i(2/\pi k_i)^{1/2}\sin(k_i r+\theta_i-\pi\nu_i) , \tag{3}$$

with

$$\theta_i=-\frac{l_i\pi}{2}+\frac{1}{k_i}\ln 2k_i r+\arg\Gamma\left[l_i+1-\frac{i}{k_i}\right] , \tag{4}$$

where $k_i=1/2\varepsilon_i^2$ denotes the momentum of the photoelectron, l_i its orbital angular momentum, and

$$\delta_{l_i}=\arg\Gamma\left[l_i+1-\frac{i}{k_i}\right]$$

the Coulomb phase shift.

When $\varepsilon_i<0$, the boundary condition at infinity requires that ν_i satisfies the following condition (in atomic units):

$$\varepsilon_i=-\frac{1}{2\nu_i^2} . \tag{5}$$

Ψ_i can be expressed in terms of the Whittaker function W as

$$\Psi_i=\chi_i(-1)^{l_i}\nu_i^{1/2}[\Gamma(\nu_i-l_i)\Gamma(\nu_i+l_i+1)]^{-1/2}\times W_{\nu_i,l_i+1/2}(2r/\nu_i) . \tag{6}$$

The *close-coupled* channel wave functions Ψ_α satisfy boundary conditions at a small distance $r=r_c$, such that the potential seen by the electron at $r\geq r_c$ can be written as $-Z/r$. They take into account the short-range interactions and are defined by

$$\Psi_\alpha=\sum_i \chi_i U_{i\alpha}(f_i\cos\pi\mu_\alpha-g_i\sin\pi\mu_\alpha) . \tag{7}$$

The matrix $U_{i\alpha}$ connects channels i to the close-coupled eigenchannels α. $\pi\mu_\alpha$ represents the phase shift due to the short-range interactions (at $r\leq r_c$). The summation is performed over the total number of independent channels $n_i(=n_\alpha)$.

Both boundary conditions are satisfied if the wave function of the system can be written as a linear combination of $(\Psi_\alpha)_{\alpha=1,n_\alpha}$ and as a linear combination of $(\Psi_i)_{i=1,n_i}$:

$$\Psi=\sum_\alpha A_\alpha\Psi_\alpha=\sum_i Z_i\Psi_i . \tag{8}$$

This leads to the following equations:

$$\sum_\alpha U_{i\alpha}\sin\pi(\nu_i+\mu_\alpha)A_\alpha=0 , \tag{9}$$

$$\sum_\alpha U_{i\alpha}\cos\pi(\nu_i+\mu_\alpha)A_\alpha=Z_i , \tag{10}$$

A nontrivial solution of Eq. (9) requires that

$$\det(F_{i\alpha})=\det[U_{i\alpha}\sin\pi(\nu_i+\mu_\alpha)]=0 . \tag{11}$$

The solution of Eqs. (11) and (5) in the discrete spectrum and comparison with experimental data allows the determination of the quantum-defect parameters $\mu_\alpha, U_{i\alpha}$. Conversely, knowledge of the quantum-defect parameter yields considerable information on the atomic spectrum: it enables one to determine the energies of high Rydberg states, and by extrapolation, the positions and line shapes of autoionizing states. An equivalent formulation[10,15,16] of Eq. (11) is

$$\det(\tan\pi\nu+\mathbf{R})=0 , \tag{12}$$

where $\tan\pi\nu$ is the diagonal matrix with elements $(\tan\pi\nu_i)_{i=1,n_i}$ and $\mathbf{R}=\mathbf{U}\tan\pi\mu\mathbf{U}^T$ is the *reaction* matrix describing the interaction of the electron with the core during the "collision." $\tan\pi\mu$ is the diagonal matrix $(\tan\pi\mu_\alpha)_{\alpha=1,n_\alpha}$.

B. MQDT wave functions

For practical reasons, we choose to express MQDT wave functions as linear combinations of the collision wave function Ψ_i (which we calculate). We distinguish three different regions.

(i) *Discrete spectrum* (all channels closed; $\varepsilon_i<0$ for all i). The normalized MQDT wave function Ψ can be written (for $r\geq r_c$) as

$$\Psi=\sum_i Z_i\Psi_i/N \ , \tag{13}$$

with[12]

$$N^2=\sum_i Z_i^2\nu_i^3+\sum_\alpha \frac{d\mu_\alpha}{d\varepsilon}A_\alpha^2 \ . \tag{14}$$

In Eq. (14), we neglect the energy dependence of the $U_{i\alpha}$ matrix.[12]

(ii) *Autoionization region* (n_ρ channels open, i.e., such that $\varepsilon_i\geq 0$). There are n_ρ independent solutions Ψ_ρ written as

$$\Psi_\rho=\sum_i Z_{i\rho}\Psi_{i\rho}/N_\rho \ , \tag{15}$$

where $\Psi_{i\rho}$ is defined by Eq. (1) with $\nu_i=-\tau_\rho$. The phase shift τ_ρ is chosen among the n_ρ possible values of the quantum defect $-\nu_j$, where j denotes an open channel. The normalization constant N_ρ is such that

$$N_\rho^2=\sum_{i,\text{open}} Z_{i\rho}^2 \tag{16}$$

and N_ρ varies strongly with energy in the vicinity of the resonances; it assures the energy normalization of the wave function.

(iii) *Continuum spectrum* (all channels open, $\varepsilon_i\geq 0$ for all i). There are n_α independent solutions which can be chosen to be the close-coupled channel wave functions Ψ_α (or any linear combination of these wave functions). In order to stress the continuity between the different energy regions [see Eqs. (13) and (15)] we write Eq. (6) as

$$\Psi_\alpha=\sum_i Z_{i\alpha}\Psi_{i\alpha} \ , \tag{17}$$

with $Z_{i\alpha}=U_{i\alpha}$ and $\Psi_{i\alpha}$ defined by Eq. (1) with $\nu_i=-\mu_\alpha$.

C. Determination of MQDT parameters

In the present work we study two- and three-photon ionization and autoionization of xenon and krypton. The types of intermediate and final states involved in these processes are indicated in Fig. 1. We need to determine the MQDT parameters for the $J=0,2$ even-parity and $J=1,3$ odd-parity Rydberg series. Each J state indicated in Fig. 1 consists of several channels converging towards

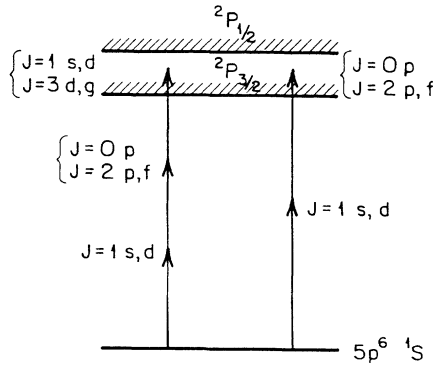

FIG. 1. Schematic representation of the energy levels and Rydberg series.

one of the two ionization thresholds $^2P_{3/2}$ or $^2P_{1/2}$. For example, the $J=2$ even-parity subset contains the four channels $[P_{3/2}]f_{7/2}$, $[P_{3/2}]f_{5/2}$, $[P_{3/2}]p_{3/2}$, $[P_{3/2}]p_{1/2}$ (in jj coupling notation) converging to the first ionization threshold and the two channels $[P_{1/2}]f_{5/2}$, $[P_{1/2}]p_{3/2}$ converging to the second ionization threshold. The $J=1$ odd-parity series in xenon and krypton have been extensively studied in the literature.[12,14,17] The $J=3$ d states of Kr have been analyzed by Aymar *et al.*,[14] in connection with detailed experimental measurements.[23] We shall therefore comment in more detail on the analysis of the $J=0,2$ even-parity states.

Since only two ionization thresholds are involved, the quantum numbers ν_i [Eq. (5)] can only take two different values $\nu_{1/2},\nu_{3/2}$. Equation (11) can be cast in the form

$$F(\nu_{1/2},\nu_{3/2})=0 \tag{18}$$

which, with $\nu_{1/2}$ defined modulo 1, determines the energy-dependent Lu-Fano plot[12] in the $(\nu_{3/2},\nu_{1/2})$ plane. Theoretical energies (in the bound spectrum) are the intersections of Eq. (18) and

$$E=I_{1/2}-1/2\nu_{1/2}^2=I_{3/2}-1/2\nu_{3/2}^2 \ . \tag{19}$$

For given J and parity, the MQDT parameters μ_α and $U_{i\alpha}$ (where μ_α is chosen to depend linearly on the energy) are determined by fitting theoretical energies to experimental energies.[23–25] In the case of the rare gases, the short-range interactions are dominated by the electrostatic interaction: the close-coupled channels α are nearly LS couples. The transformation matrix $U_{i\alpha}$ is therefore expressed as

$$U_{i\alpha}=\sum_{\bar\alpha} U_{i\bar\alpha}V_{\bar\alpha\alpha} \ , \tag{20}$$

where $\bar\alpha$ represents the LS-coupled channels, $U_{i\bar\alpha}$ is the jj-LS transformation matrix, and $V_{\bar\alpha\alpha}$ describes the deviation of the "true" close-coupled wave functions from pure LS coupling due to spin-orbit interaction or configuration mixing (e.g., between $p^5p\ ^1D_2$ and $p^5f\ ^1D_2$). $V_{\bar\alpha\alpha}$ is usually expressed as a product of rotation matrices.

When a large number of channels is involved (e.g., six in the $J=2$ case), and when available experimental data

are scarce, fitting of energy levels may lead to several sets of parameters; it is essential to use all possible information on the dynamics of the multielectron interaction in order to determine uniquely these parameters. A first difficulty is to assign the parameters μ_α (whose first estimation can be determined on the Lu-Fano plot[12]) to the corresponding LS-coupled channels. Consider, for example, the $J=2$ p states. The energy splitting for the different LS term involved can be expressed as a function of Slater integrals:

$$E(^3P)-E(^3D)=\tfrac{6}{25}F^2(5p,np)\ , \tag{21}$$

$$E(^1D)-E(^3D)=\tfrac{12}{25}G^0(5p,np)\ . \tag{22}$$

Since $G^0 \ll F^2$ (which has been verified by an independent calculation), this leads us to assume that $E(^3P)>E(^1D)>E(^3D)$ and that the quantum defects $\mu(^{2S+1}L)$ vary in the opposite order. This ordering of the μ_α parameters will be true as long as the spin-orbit interaction (inside the core) is smaller than the electrostatic interaction and that the channel mixing is not too important.

A useful check on the accuracy of the MQDT parameters obtained by fitting the energy levels is to calculate the admixture coefficients Z_i [Eq. (8)] in the Jl coupling scheme and to verify that the assignment of the excited states by the MQDT fitting procedure corresponds to the experimental assignment (allowing some exceptions in the vicinity of perturbing states). We found that Jl coupling is in general more appropriate for the characterization of high Rydberg states than jj coupling. This is particularly true for high angular momentum states and can be understood on simple physical grounds: The electron remains most of the time far from the core region; its spin-orbit interaction is very weak, since this effect varies in $1/r^3$. The dominant coupling is then the coupling between the orbital momentum of the electron (l) and the total angular momentum of the core (J).

Finally, as pointed out by Aymar,[26] there remains an indeterminacy in the matrix $U_{i\alpha}$ (more precisely in the sign and also amplitude of some coefficients of the $V_{\bar{\alpha}\alpha}$), which cannot be lifted by fitting energy levels only. We note that this work will simulate further experiments on the spectroscopy of even-parity states of the rare gases which could enable us to lift this indeterminacy. Let us point out, however, that in the cases investigated in this work, the $U_{i\alpha}$ matrix does not differ much from the jj-LS transformation matrix; the (dipole) interaction between s and d states ($J=1$) is rather weak; the quadrupole interaction between p and f states ($J=2$) is even more reduced. Thus the possible inaccuracy in some of the coefficients of the MQDT wave functions, due to lack of information, should not affect much the final result.

The optimal parameters obtained for the $J=0$ and 2 even-parity states in Xe and Kr are indicated in Tables I and II. [For completeness, we also indicate in Table III the parameters for the $J=3$ (d states) in Xe; the other sets of parameters can be found elsewhere.[12,14,17]] In Figs. 2 and 3 we present the corresponding Lu-Fano plots for Xe and Kr. Some low-lying states ($6p$ in Xe and $5p$ in Kr) have not been included in the fitting procedure. Some information about the importance of channel interaction can be deduced in a simple way[16] from the Lu-Fano plot. The gaps between the different branches at the crossings can be related to the coupling strength between the different channels. In Figs. 2 and 3 these gaps are rather small and the branches are nearly at right angles (especially for Kr). This confirms that the channel mixing is not very pronounced. It is in particular reduced compared to odd-parity spectra.[12,14,17]

Around $\nu_{3/2}=2$ and 3, the Lu-Fano plot exhibits spurious branches due to the presence of (artificial) states $^2P_{1/2}2f$, $^2P_{1/2}3f$. This problem, previously noted by Seaton,[10] can be solved by replacing Eq. (11) or (12) by the equivalent form

$$\left[\frac{\tan\pi\nu}{A}+Y\right]=0\ , \tag{23}$$

the factor $A=A(\varepsilon,l)=\prod_{p=0}^{l}(1+p^2\varepsilon)$ removing the spurious roots.[27] In the present approach we shall simply remove the artificial states and extrapolate the Lu-Fano plot in the region $\nu_{3/2}=2$ and 3 [Figs. 2(a) and 3(a)], which leads practically to the same result.

Finally, the experimental results of Pratt and coworkers show evidence of some autoionizing $^2P_{1/2}g$ ($J=3$) states in Xe and Kr.[2,3] There are no experimental data on $^2P_{1/2}g_{7/2}$, $^2P_{3/2}g_{9/2}$, $^2P_{3/2}g_{7/2}$ energy levels. Note that these states are almost hydrogenic, with very small quantum defects. In order to be able to qualitatively compare with the results obtained by Pratt and coworkers,[2,3] we have introduced g and g' states in our calculation in the following way. The channel with the highest energy (^1P) has a zero quantum defect. The other channels have quantum defects corresponding to the energy difference with the ^1P channel, calculated by using hydrogenic wave functions and scaled by the factor $1/\pi\nu^3$. The $U_{i\alpha}$ restricted to g states is the jj-LS transformation matrix. Finally, we introduce a small interaction between g and d ($J=3$) states in order to allow g' autoionizing states to decay into the d continuum channels. Note that this decay is anyway extremely weak.

In conclusion, we would like to point out that it is essential to have some physical insight about the values of the MQDT parameters $\mu_\alpha, U_{i\alpha}$ in order to get realistic results by fitting experimental energy values. In the present work we have performed calculations using single-configuration Hartree-Fock wave functions for p and d states and hydrogenic wave functions for f and g states in order to get some information about the quantum defects and coupling strengths. This information could also be inferred from additional experimental data.

D. Dipole matrix elements and multiphoton ionization cross sections

Following Geiger,[17] we determine dipole matrix elements from the ground state $5p^6\,^1S_0$ to $J=1$ excited states by fitting oscillator strengths in the discrete spectrum. The oscillator strength to a particular bound state is given by (in atomic units)

$$f=\frac{2E}{N^2}\left[\sum_\alpha D_\alpha A_\alpha\right]^2\ , \tag{24}$$

TABLE I. Multichannel-quantum-defect parameters for $J=2$ even-parity (p and f) states in Kr and Xe.

	α	$f\,^3F$	$f\,^1D$	$f\,^3D$	$p\,^3P$	$p\,^1D$	$p\,^3D$
	i	$P_{1/2}f_{5/2}$	$P_{3/2}f_{7/2}$	$P_{3/2}f_{5/3}$	$P_{1/2}p_{3/2}$	$P_{3/2}p_{3/2}$	$P_{3/2}p_{1/2}$
Kr	μ_α^0	−0.009	0.023	0.028	0.585	0.609	0.666
	μ_α^1	0.076	0.089	0.017	0.061	0.088	−0.013
	$U_{i\alpha}$	0.687	0.612	0.399	−0.004	−0.008	−0.008
		−0.218	0.696	−0.684	0.0	0.004	0.006
		−0.693	0.383	0.610	0.0	−0.009	−0.006
		0.003	0.0	0.002	0.395	−0.566	0.723
		0.002	0.005	0.006	0.860	0.504	−0.075
		0.0	0.005	0.015	−0.322	0.652	0.686
Xe	μ_α^0	0.013	0.032	0.041	0.494	0.557	0.623
	μ_α^1	0.020	−0.001	0.060	0.134	0.074	0.063
	$U_{i\alpha}$	0.650	0.605	0.458	0.0	−0.037	0.026
		−0.231	0.731	−0.639	0.0	−0.044	−0.036
		−0.724	0.309	0.615	0.0	−0.019	0.034
		0.0	−0.023	−0.050	0.227	−0.377	0.897
		0.0	0.036	−0.003	0.802	0.595	0.048
		0.0	0.043	−0.024	−0.553	0.708	0.437

where the close-coupled dipole matrix elements D_α can be deduced from the dipole matrix elements in LS coupling $D_{\bar{\alpha}}$,

$$D_\alpha=\sum_{\bar{\alpha}} V_{\alpha\bar{\alpha}}D_{\bar{\alpha}} \ . \tag{25}$$

$(D_{\bar{\alpha}})_{\bar{\alpha}=1,n_\alpha}$ are determined by fitting oscillator strengths calculated through Eqs. (24) and (25), to experimental oscillator strengths.[17,28,29] In the autoionization region the density of oscillator strength is given by

$$\frac{df}{dE}=2E\sum_{\rho=1}^{n_\rho}\left[\sum_\alpha D_\alpha A_\alpha^\rho\right]^2\Big/N_\rho^2 \ . \tag{26}$$

We check that we obtain good agreement with experimental values[28] and other theoretical[12,14,22] calculations for Xe and Kr. In Sec. III, we present some one-photon autoionization profiles.

Dipole matrix elements between excited states are defined by

$$D_{fi}=\langle f|\boldsymbol{\varepsilon}\cdot\mathbf{r}|i\rangle \ , \tag{27}$$

where $\boldsymbol{\varepsilon}$ is the polarization of the radiation field which, in the present work, is chosen to be linear. $\langle f|\mathbf{r}\rangle=\Psi_f$, $\langle i|\mathbf{r}\rangle=\Psi_i$ are MQDT wave functions [see, e.g., Eqs. (13), (15), or (17); we limit ourselves to the calculation of bound-bound and bound-free dipole matrix elements].

Ψ_i and Ψ_f are determined only outside the core ($r\geq r_c$). We use the Burgess-Seaton cutoff procedure[30] to eliminate the well-known divergence near the origin, by introducing

$$\Psi_i\rightarrow\Psi_i\{1-\exp[10r/l_i(l_i+1)]\}^{2l_i+1} \ . \tag{28}$$

We check that the final result does not depend on $r_c[=l(l+1)/10$ a.u.].

The N-photon generalized ionization cross section to lowest-order perturbation theory is defined as

$$\sigma_N=2\pi\left[\frac{\alpha c}{a_0}\right]\left[\frac{\omega}{F_0}\right]^N\sum_J\sum_{\alpha=1}^{n_\alpha}|D_\alpha^N|^2 \ . \tag{29}$$

σ_N is expressed in $\mathrm{cm}^{2N}\mathrm{s}^{N-1}$ units. α (in the parentheses) is the fine-structure constant, c the speed of light, and a_0 the Bohr radius. ($\alpha c/a_0$ is 1 s^{-1} in atomic units.) ω is the photon energy (a.u.). $F_0=3.22\times10^{34}$

TABLE II. MQDT parameters for $J=0$ p states in Kr and Xe.

	α	$p\,^1S$	$p\,^3P$
	i	$P_{1/2}p_{1/2}$	$P_{3/2}p_{3/2}$
Kr	μ_α^0	0.461	0.585
	μ_α^0	0.425	0.329
	$U_{i\alpha}$	0.465	0.885
		0.885	−0.465
Xe	μ_α^0	0.417	0.572
	μ_α^1	0.051	0.152
	$U_{i\alpha}$	0.330	0.944
		0.944	−0.330

TABLE III. MQDT parameters for $J=3$ odd-parity states in Xe.

	α	$d\,^3F$	$d\,^1F$	$d\,^3G$
	i	$P_{1/2}f_{5/2}$	$P_{3/2}d_{5/2}$	$P_{3/2}d_{3/2}$
Xe	μ_α^0	0.497	0.379	0.356
	μ_α^1	0.024	0.012	0.011
	$U_{i\alpha}$	0.623	−0.634	0.460
		−0.082	0.528	0.845
		0.778	0.564	−0.278

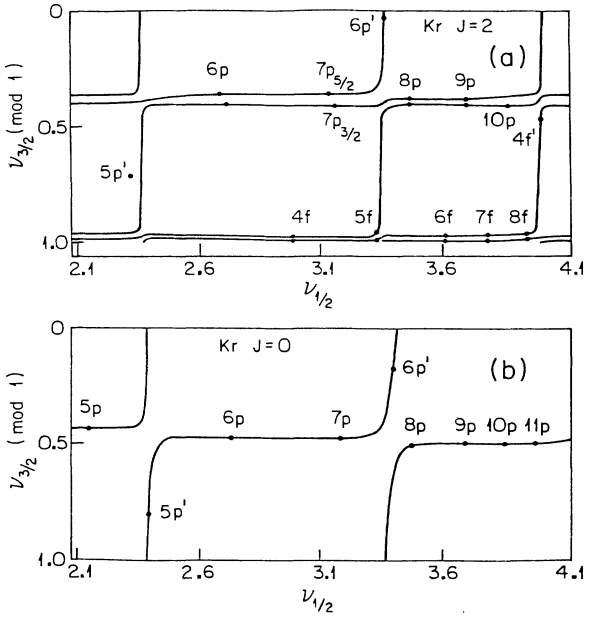

FIG. 2. Three stages of the plasma-vacuum interface development under the influence of the Rayleigh-Taylor instability of a thin plasma layer above a vacuum and limited from above by a rigid wall. Here we have taken $\alpha=\exp(\gamma t)/4$; $\gamma t=0, 1.5, 1.75$.

photons/cm^2 s. There is a double summation on the total angular momentum of the final state (J) and on the number of open channels n_α (or n_ρ in the autoionization region) for each J. Finally, the N-photon ionization amplitude D_α^N is defined by

$$D_\alpha^N=\sum_{m,n,p}\frac{\langle\alpha|\boldsymbol{\varepsilon}\cdot\mathbf{r}|m\rangle\langle m|\boldsymbol{\varepsilon}\cdot\mathbf{r}|n\rangle\cdots\langle p|\boldsymbol{\varepsilon}\cdot\mathbf{r}|i\rangle}{[E_m-E_i-(N-1)\omega]\cdots(E_p-E_i-\omega)}\ . \tag{30}$$

In the present work we limit the summation over intermediate states in Eq. (30) to the discrete spectrum. We sum up to about 25 Rydberg states, in order to obtain reasonable convergence of the series. Since we investigate two- or three-photon ionization processes near the threshold (more precisely between the two threshold and slightly above the second ionization threshold), the energy corresponding to the absorption of the next to the last photon remains below the first excited state (both in Xe and Kr). The discrete part of the spectrum gives the most important contribution to the summation and the approximation made by truncating the series should yield reasonable cross sections in this energy range. Note that summing over the whole spectrum in the MQDT formalism is by no means a simple problem, which goes beyond the scope of the present paper.

E. Photoelectron angular distributions

In order to calculate photoelectron angular distributions,[31,32] we use the incoming-wave normalization for the final-state wave function, expanded as follows:

$$|f_{m_s,m_{J_c},J_c}(\mathbf{k},\mathbf{r})\rangle=\sum_{l,m_l}i^l e^{-i\delta_l}Y^*_{lm_l}(\hat{k})\sum_{j,J,\alpha}e^{-i\pi\mu_\alpha}(\alpha|J_c jJM_J)(J_c jJM_J|J_c m_{J_c}jm_j)(J_c m_{J_c}jm_j|lm_l sm_s)|\alpha\rangle\ . \tag{31}$$

δ_l is the Coulomb phase shift, $\mathbf{k}$ the momentum of the photoelectron. $\hat{k}=(\theta,\varphi)$ characterizes the direction of the outgoing electron by reference to the polarization axis (for linear polarization) or by reference to the propagation axis (circular polarization). The collision channels (i) are here identified by the set of quantum numbers $\{J_c jJM_J\}$ (jj coupling). In the open continuum, $(\alpha|J_c jJM_J)=(\alpha|i)=U^T_{\alpha i}$; the other coefficients in Eq. (31) are usual Clebsch-Gordan coefficients.

The N-photon partial ionization amplitude can be written as

$$M^N(\hat{k})[m_s,m_{J_c},J_c]=\sum_{lm_l jJ\alpha}i^l(-1)^{(1/2)-m_j-j+J_c-M_J}e^{i\delta_l+i\pi\mu_\alpha}Y_{lm_j}(\hat{k})[(2j+1)(2J+1)]^{1/2}$$

$$\times\begin{bmatrix}l & s & j\\ m_l & m_s & -m_j\end{bmatrix}\begin{bmatrix}j & J & J\\ m_j & m^c_{J_c} & -M_J\end{bmatrix}Z_{i\alpha}D^N_\alpha\ . \tag{32}$$

For the sake of generality, we do not make here any distinction between the open continuum (all channels open; $Z_{i\alpha}=U_{i\alpha}$) and the autoionization region [$\alpha\to\rho$; $\mu_\alpha\to\tau_\rho$; $Z_{i\rho}$ is defined by Eq. (8)]. In the latter case, J_c can only take one value ($\frac{3}{2}$).

Finally, the N-photon differential ionization cross section is given by

$$\frac{d\sigma_N^{(J_c)}}{d\Omega}=2\pi\left[\frac{\alpha c}{a_0}\right]\left[\frac{\omega}{F_0}\right]^N\times\sum_{m_s,m_{J_C}}|M^N(\hat{k})[m_s,m_{J_c},J_c]|^2\ . \tag{33}$$

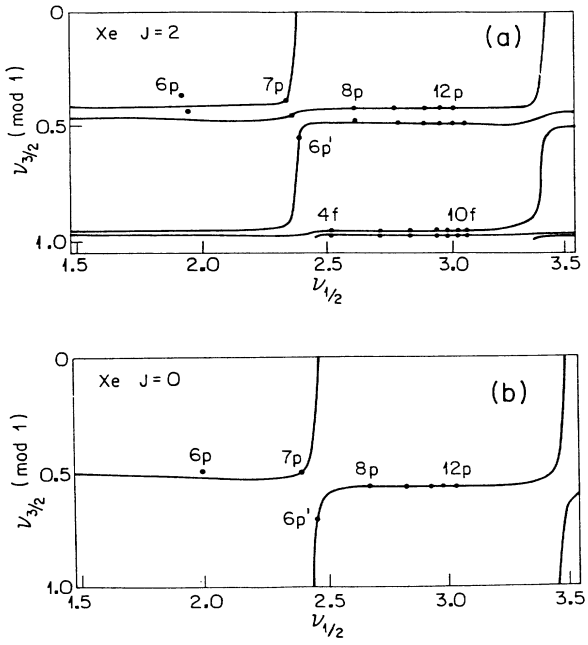

FIG. 3. Energy-dependent Lu-Fano plot for $J=2$ (a) and $J=0$ (b) xenon bound states.

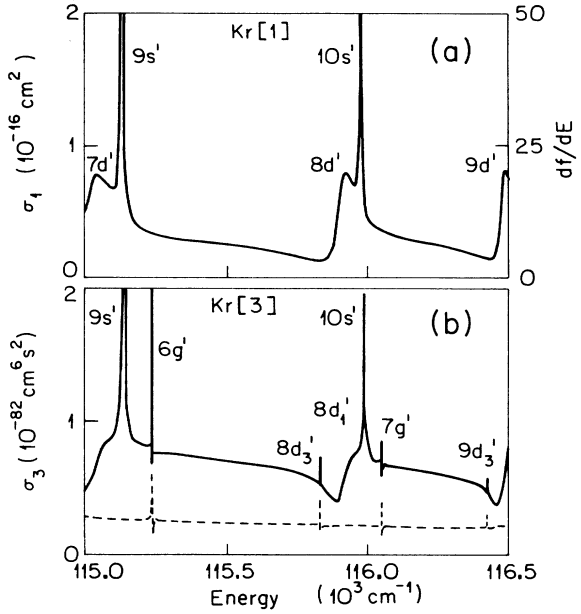

FIG. 4. Autoionization spectra in Kr. (a) Density of one-photon oscillator strength and photoionization cross section. (b) Three-photon ionization (——) total cross section, (— — —) $J=3$ partial cross section.

In the following we present some applications of the method exposed in this section.

III. RESULTS AND DISCUSSION

A. Autoionization spectra

In Figs. 4–6 we present some autoionization spectra in Kr and Xe corresponding to absorption of one to three photons. The number of photons involved is indicated in brackets in the figures. The energy range, 115 000–116 500 cm^{-1} in Kr, and 103 000–106 000 cm^{-1} in Xe, is chosen for illustration purposes, more than because of any numerical limitation. In Figs. 4(a) and 5(a) we indicate both the one-photon ionization cross section (in cm^2) and the density of oscillator strength df/dE, so that the reader may directly compare these results to experimental measurements[26] or other theoretical calculations.[13] For two-photon (Fig. 6) and three-photon [Figs. 4(b) and 5(b)] ionization, we express the ionization cross sections in the usual cm^{2n} s^{N-1} units [see Eq. (29)].

Figure 6 shows two-photon autoionization spectra in Kr [Fig. 6(a)] and in Xe [Fig. 6(b)]. The autoionizing resonances which appear in the spectra are indicated in the figure. The primes indicate that the ion is in the $P_{1/2}$ state. The solid line is the total ionization cross section. The dashed line shows the partial cross section corresponding to the transitions to $J=0$ final states. This contribution is much smaller (by about a factor of 30) than that of the $J=2$ states, except, of course, in the vicinity of the $J=0$ resonances. Finally, the cross in Fig. 6(a) indicates the experimental measurement of the two-photon ionization cross section by McCown *et al.*,[33] in good agreement with the present calculation.

In Figs. 4(b) and 5(b) we present three-photon autoionization spectra and we compare them to the one-photon autoionization spectra in Figs. 4(a) and 5(a), involving the same ($J=1$) autoionization resonances. As in two-photon autoionization, the solid line is the total ionization cross section. The dashed line is the $J=3$ partial cross section. In contrast to the $J=1$ partial cross section, the $J=3$ cross section is almost flat. The sharp $J=3$ resonances nearly do not interact with the adjacent continua.

The $J=1$ three-photon autoionization resonances

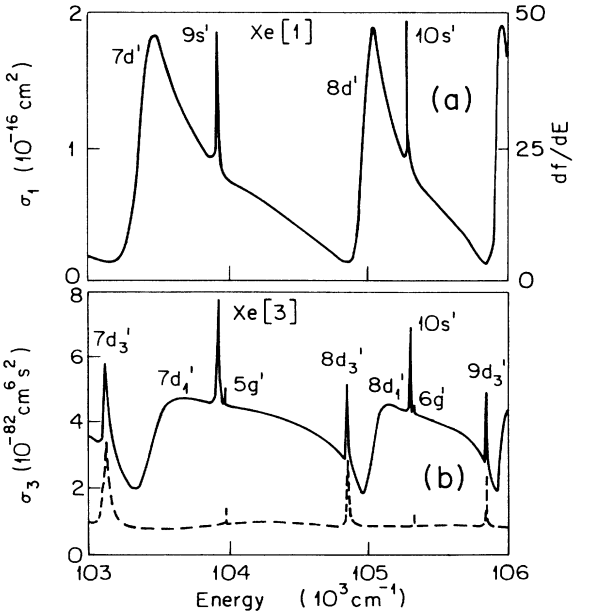

FIG. 5. Autoionization spectra in Xe. Same as in Fig. 4.

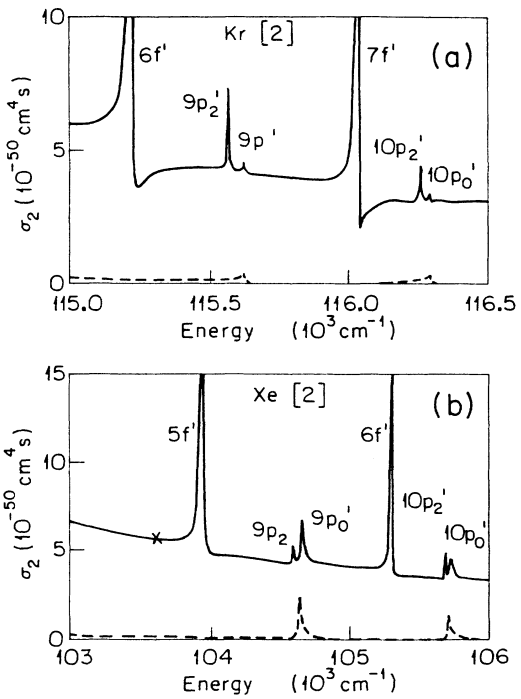

FIG. 6. Two-photon autoionization spectra in Kr (a) and in Xe (b). ——, total ionization cross section; — — —, $J=0$ ionization cross section. ×, experimental point by McCowen *et al.* (Ref. 33).

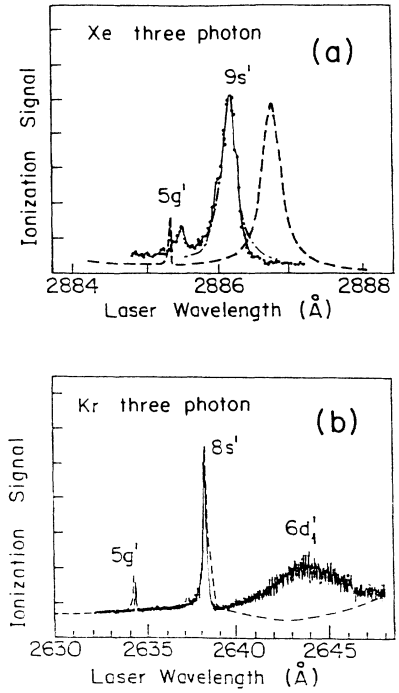

FIG. 7. Comparison with experimental data in Xe (a) (Ref. 2) and Kr (b) (Ref. 3). ——, experimental data; — — —, present work; —·—·—·, calculated $9s'$ Xe resonance supposed with the experimental peak.

show some similarity with the $J=1$ one-photon resonances: the symmetries are the same and the widths comparable. The line shapes are, however, different. In fact, since the matrix elements involved in one-photon absorption are different from those in three-photon absorption, one should not expect much resemblance between one- and three-photon autoionization line shapes.

In conclusion, let us comment on the evolution of an autoionization spectrum as the number of photons absorbed to reach these states increases, or more significantly, as the total angular momentum J of the final state increases. What is obvious from the spectra in Figs. 4(a), 6(a), and 4(b) (dashed line) and also in Figs. 5(a), 6(b), and 5(b) (dashed line), is that autoionization processes become less and less important as J increases: the interaction between the channels decreases from $J=1$ to 3. This is due to the nature of the electron-electron interaction (involving higher multipoles for $J=2,3$). The highest angular momentum states remain mainly outside the core and therefore do not interact much.

B. Comparison with experimental autoionization spectra (Refs. 2 and 3)

In Fig. 7 we compare the results of our calculation (dashed line) to experimental measurements (solid line) of three-photon autoionization in Xe [Fig. 7(a)] and Kr [Fig. 7(b)]. The vertical scale has been chosen in order to match the background and the maximum of the s' state ($9s'$ in Xe, $8s'$ in Kr). No adjustment has been made for the horizontal scale.

Figure 7(a) shows good agreement between our result and the experimental data.[3] The calculated $9s'$ peak is slightly displaced, by about 1.5 Å, i.e., 18 cm^{-1}. If we superpose the theoretical and experimental maxima (dot-dashed line), we obtain a good agreement for the width and the line shape of the resonance.

The comparison in Kr (Ref. 3) shown in Fig. 7(b) is less satisfactory. There is good agreement for the $5g'$ and $8s'$ peaks, but the $6d'$ resonance, as produced in our calculation, appears to be very broad, spread over a much larger wavelength range than in the experiment. We tried changing some of the MQDT parameters involved in the description of this state (in particular, those which are not unambiguously determined; see Sec. II) without any improvement. This discrepancy may be due to the truncated summation, or, more generally, to the various approximations inherent in our calculation. Autoionization is a very subtle effect, resulting from an interference between different paths leading to the same final state: if the respective amplitudes for these processes are not accurately determined, the resulting line shape may be quite different from the actual one. This would be especially true for broad states such as the $6d'$.

C. Photoelectron angular distributions

We have determined photoelectron angular distributions for three-photon absorption to the $9s'$ and $7d'$ autoionizing states in Kr and Xe and we compare them in Figs. 8 and 9 to experimental measurements performed by Pratt and co-workers.[2,3] The experimental data are indicated by the closed circles. The solid line is the best fit with the data.[2,3] Our result is shown by the dashed

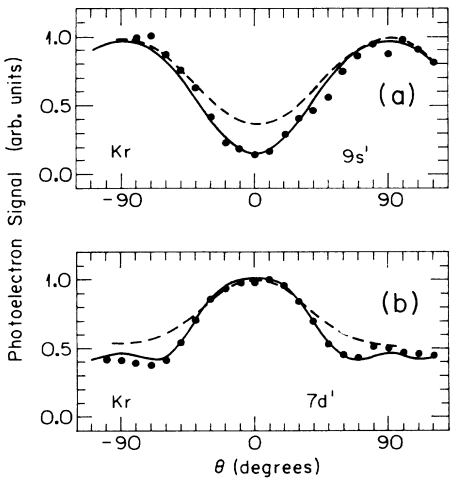

FIG. 8. Photoelectron angular distributions for three-photon autoionization to the $9s'$ (a) and the $7d'$ (b) states in Kr. ●, experimental data; ——, best fit with experimental data (see Ref. 3). — — —, present work.

line. The distributions have been vertically matched at the maximum.

Photoelectron angular distributions involve the addition of all *amplitudes* of the transitions leading to different final states [see Eqs. (32) and (33)]. It is therefore a very sensitive test to any theoretical calculation and even a partial agreement with experimental observations should be considered as satisfactory. A good agreement is obtained in Kr (Fig. 8). It is not as good for the $7d'$ state in Xe [Fig. 9(b)], since the calculation is not able to reproduce the increase at 90°. Finally, the angular distributions for the $9s'$ Xe state [Fig. 9(a)] are substantially different. We do not understand the exact reason for this discrepancy. One possibility is that the approximation which consists in neglecting the small-r region (by introducing a cutoff) may not be valid for s wave functions, which have a non-negligible amplitude near the origin.

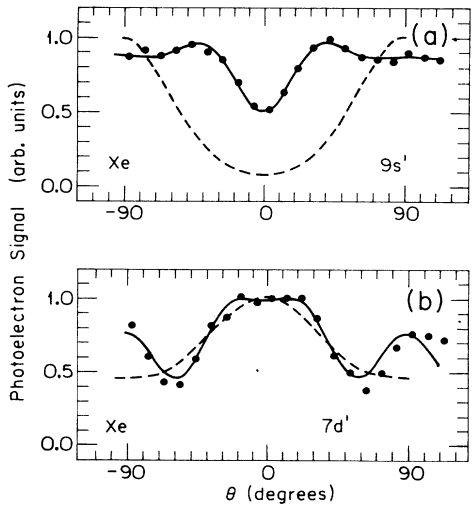

FIG. 9. Same as Fig. 8 for xenon (see Ref. 1).

But again, why does the $9s'$ state of Kr not present the same problem?

D. Two-photon ionization above the second ionization threshold

Finally, we have also calculated two-photon ionization above the second ionization threshold, up to about 130 000 cm^{-1} in Xe, and 140 000 cm^{-1} in Kr, before the first intermediate resonance. We represent these cross sections in Fig. 10 (solid line), together with other calculations.[8,18,34] The crosses indicate the MQDT result obtained by Gangopadhyay *et al.*[18] The difference between these two results comes from the more accurate MQDT analysis in the present work and the different method for calculating the first photon absorption. We used fitted one-photon oscillator strengths. Gangopadhyay *et al.* calculated these oscillator strengths by using a quantum-defect ground-state wave function.

The only other extensive calculations in the rare gases are those of McGuire,[34] represented in Fig. 10 by the dashed line. These results are always higher than our cross sections. McGuire uses an independent-electron approximation. Introduction of the electron-electron interaction in the description of MPI of the rare gases reduces the cross sections.[8] In Fig. 10(a) we have also represented (short-dashed line) the random-phase approx-

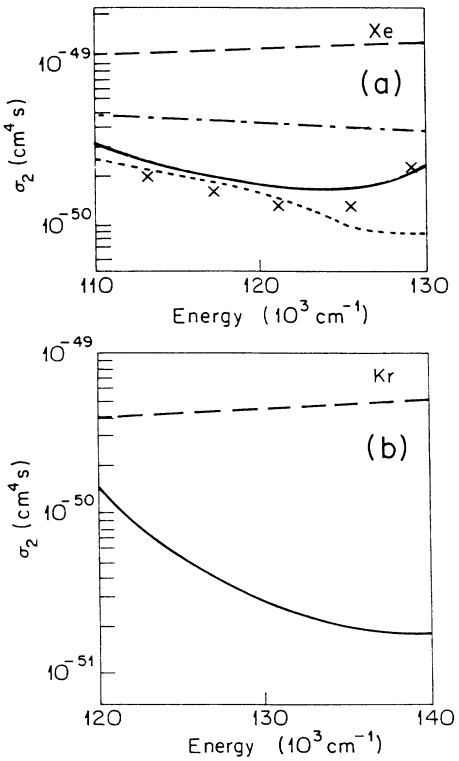

FIG. 10. Two-photon ionization above the second ionization limit in Xe (a) and Kr (b). ——, present work; ×, MQDT result by Gangopadhyay *et al.* (Ref. 18); — — —, independent-electron calculation of McGuire (Ref. 34); —·—·—·, random-phase-approximation exchange (RPAE) result of L'Huillier and Wendin (Ref. 8); ----, linear RPAE result of L'Huillier and Wendin (Ref. 8) (without double excitations; see Ref. 8).

imation (RPA) result of L'Huillier and Wendin.[8] This result (which does not include the fine-structure splitting) lies slightly below the present calculation. This is to be expected, since the RPA result also includes double excitation effects, such that one photon excites one electron, a second photon excites a second electron.[8,9] These effects will further reduce the cross sections. Part of them may be inherently included in the MQDT which uses experimental energies and oscillator strengths. However, no double excitations are introduced in the fitting of energy levels nor in the diagonalization of the collision channels. We would therefore expect the MQDT result to be closer to the intermediate result obtained by L'Huillier and Wendin[8] (dot-dashed line), without these effects. The calculations to which we compare are, however, extremely different, both of them involving significant approximations. It is then difficult to attribute any differences to specific physical effects included or not included in the different approaches, more than to the inaccuracy due to the numerical approximations. The overall agreement can be considered as satisfactory. It emphasizes that independent-electron approximations cannot correctly describe the dynamics of a MPI process in the rare gases.

Finally, we have also calculated three-photon ionization above the second ionization limit. Our results are within 20% of those obtained by McGuire.[34] For example, at 266 nm, we have $\sigma_3 = 6 \times 10^{-82}$ cm^6 s^2. The result of McGuire[34] is 5×10^{-82} cm^6 s^2. Perry and Landen[35] have measured $\sigma_3 = 1.2 \times 10^{-82}$ cm^6 s^2. Kulander[7] calculates a cross section equal to 2.5×10^{-82} cm^6 s^2. All of these results are in reasonable agreement. We, however, believe that McGuire's results may be slightly too high, because of the independent-electron approximation. In our calculation the error may be due to the truncated summation approximation, which may become worse as the number of photons increases.

The present results are also in reasonable agreement with earlier results by Gangopadhyay *et al.*[18] As given in Ref. 18, the results for three-photon ionization appear to differ by six orders of magnitude. This difference, however, has been traced to an error in the coefficient converting energy units from a.u. to eV.

IV. CONCLUSIONS

In closing, we would like to discuss the potential of MQDT in the description of multiphoton ionization spectra, as well as the limitations of the present approach.

Multichannel-quantum-defect theory allows one to take into account various intrachannel and interchannel interactions between different Rydberg series. The notion of "state" or "configuration" is replaced in this formalism by the more powerful concept of "channel." Instead of "configuration mixing" (i.e., for each state of a particular channel), one talks about "channel mixing." The effect of spin-orbit interaction, for both the core and the outer electron, is taken into account by considering *jj*-coupled channels converging to different thresholds (separated in energy by the fine-structure splitting) and coupled via the electron-electron interaction. The semiempirical approach which is based on fitting experimental data provides a very accurate description of the atomic structure. MQDT is very well adapted to the description of properties of high Rydberg states and, in particular, autoionization profiles. This is especially important for complex systems such as the heavy rare gases, where other (*ab initio*) theoretical approaches become impractical for the description of the details concerning the spectroscopic and dynamic properties of the atom.

On the other hand, MQDT, in the form employed in this work, is less accurate in the description of the ground state and perhaps some of the low-lying excited states which often are excluded from the fitting procedures as implemented here. It is, however, possible to circumvent such limitations in accuracy by combining MQDT with *ab initio* calculations as obtained, for example, through R-matrix[21,22] or relativistic RPA (Ref. 20) approaches.

The important question, in the present context, is to what extent this theory can be applied to multiphoton ionization problems. The main advantage is that it gives an extremely accurate description of the atomic spectrum. This is very useful for the description of resonant processes in the discrete spectrum or in an autoionizing region, since the positions of the states need to be precisely determined. And it provides a good description of the dynamics of complex atomic systems.

As we have emphasized in this paper, the summation over intermediate states poses a different problem. The approximation consisting in limiting this summation to the discrete spectrum is probably reliable before the minimum between the first and the second intermediate resonance, and for a small number of photons absorbed. Dalgarno-Lewis types of procedures[36] cannot be used in a simple way. One solution might be to perform the summation explicitly[8] or to combine the Green's-function techniques developed in single-channel quantum-defect theory with additional information obtained from the MQDT analysis. We shall deal with this problem in the near future.

In conclusion, we think that multichannel-quantum-defect theory can be a useful tool for the realistic incorporation of atomic structure in the description of multiphoton processes, especially if the limitations mentioned above can be removed. In the present work we have applied MQDT to calculations of two- and three-photon ionization and autoionization processes in Xe and Kr. We found satisfactory agreement with experimental data[2,3] and other theoretical calculations.[7,8,34] We are also in the process of applying this technique to the investigation of other multiphoton absorption processes,[4,5] which will be presented in forthcoming publications.

Our earlier incomplete analysis[18] stimulated a few experiments which have proven quite valuable to us in this work. We present our new results—which still contain loose ends—with the hope and appeal for further experimental input. The complexity that makes multiphoton calculations difficult and demanding has a positive side. It probes the dynamics of a multielectron atom at a level not accessible and complementary to single-photon absorption; which, in our view, makes the whole effort very worthwhile.

ACKNOWLEDGMENTS

We would like to thank Dr. W. E. Cooke and Dr. T. N. Chang for very helpful discussions. This work has been supported in part by the National Science Foundation, under Grant No. PHY-83-06263 and in part by the U.S. Department of Energy, Grant No. DE-FG03-87ER60504.

*Permanent address: Service de Physique des Atomes et des Surfaces, Centre d'Etudes Nucléaires de Saclay, 91191 Gif-sur-Yvette, France.

[1]P. R. Blazewicz, J. A. D. Stockdale, J. C. Miller, T. Efthimiopoulos, and C. Fotakis, Phys. Rev. A **35**, 1092 (1987).

[2]J. L. Dehmer, S. T. Pratt, and P. M. Dehmer, Phys. Rev. A **36**, 4494 (1987).

[3]S. T. Pratt, P. M. Dehmer, and J. L. Dehmer, Phys. Rev. A **35**, 3793 (1986).

[4]O. L. Landen, M. D. Perry, and E. M. Campbell, Phys. Rev. Lett. **59**, 2558 (1988).

[5]M. H. R. Hutchinson and K. M. M. Ness, Phys. Rev. Lett. **60**, 105 (1988).

[6]See articles in *Multiphoton Processes,* proceedings of the 4th International Conference on Multiphoton Processes, Boulder, Colorado, 1987, edited by S. J. Smith and P. L. Knight (Cambridge University Press, Cambridge, England, 1988).

[7]K. C. Kulander, Phys. Rev. A **36**, 2726 (1987); (unpublished).

[8]A. L'Huillier and G. Wendin, J. Phys. B **20**, L37 (1987); Phys. Rev. **36**, 4747 (1987).

[9]A. F. Starace and T. F. Jiang, Phys. Rev. A **36**, 1705 (1987).

[10]M. J. Seaton, Proc. Phys. Soc. London **88**, 801 (1966); Rep. Prog. Phys. **46**, 167 (1983).

[11]U. Fano, Phys. Rev. **2**, 353 (1970).

[12]K. T. Lu, Phys. Rev. A **4**, 579 (1971); C. M. Lee and K. T. Lu, Phys. Rev. A **8**, 1241 (1973).

[13]A. F. Starace, J. Phys. B **6**, 76 (1973).

[14]M. Aymar, O. Robaux, and C. Thomas, J. Phys. B **14**, 4255 (1981).

[15]W. E. Cooke and C. L. Cromer, Phys. Rev. A **32**, 2725 (1985).

[16]A. Giusti-Suzor and U. Fano, J. Phys. B **17**, 215 (1984).

[17]J. Geiger, Z. Phys. A **282**, 129 (1977).

[18]P. Gangopadhyay, X. Tang, P. Lambropoulos, and R. Shakeshaft, Phys. Rev. A **34**, 2998 (1986).

[19]O. Robaux and M. Aymar, Comput. Phys. Commun. **25**, 223 (1982); the program has been adapted to our computer (VAX) and extended so as to handle four channels converging to the first ionization threshold.

[20]C. M. Lee, Phys. Rev. A **10**, 584 (1974); W. R. Johnson, K. T. Cheng, K. N. Huang, and M. Le Dourneuf, *ibid.* **22**, 989 (1980).

[21]M. Aymar, E. Luc-Koenig, and S. Watanabe, J. Phys. B **20**, 4325 (1987).

[22]C. Greene and L. Kim, Phys. Rev. A **36**, 2706 (1987).

[23]C. Delsart, J. C. Keller, and C. Thomas, J. Phys. B **14**, 3355 (1981); **14**, 4241 (1981); K. Yoshino and Y. Tanaka, J. Opt. Soc. Am. **69**, 159 (1979).

[24]C. E. Moore, *Atomic Energy Levels,* Natl. Bur. Stand. (U.S.) Circ. No. 467 (U.S. GPO, Washington, D.C., 1952), Vol. 2; Vol. 3 (1958).

[25]K. Yoshino and D. E. Freeman, J. Opt. Soc. Am. B **2**, 1268 (1985).

[26]M. Aymar, Phys. Rep. **110**, 163 (1984).

[27]W. E. Cooke, A. L'Huillier, and X. Tang, Bull. Am. Phys. Soc. **33**, 1040 (1988).

[28]A. Delâge and J. D. Carette, Phys. Rev. A **14**, 1345 (1976).

[29]F. Schafers, G. Schonhense, and U. Heinzmann, Phys. Rev. A **28**, 802 (1983).

[30]A. Burgess and M. Seaton, Mon. Not. R. Astron. Soc. **120**, 191 (1960).

[31]S. N. Dixit and P. Lambropoulos, Phys. Rev. A **27**, 861 (1983); T. Olsen, P. Lambropoulos, S. E. Wheatley, and S. P. Rountree, J. Phys. B **11**, 4167 (1978).

[32]D. Dill, Phys. Rev. A **7**, 1976 (1973).

[33]A. W. McCown, M. N. Ediger, and J. G. Eden, Phys. Rev. A **26**, 3318 (1982).

[34]E. J. McGuire, Phys. Rev. A **24**, 835 (1981).

[35]M. D. Perry and O. L. Landen (unpublished).

[36]A. Dalgarno and J. T. Lewis, Proc. R. Soc. London Ser. A **233**, 70 (1955).